Clim Dyn
DOI 10.1007/s00382-009-0728-z

Further analysis of singular vector and ENSO predictability in the Lamont model—Part II: singular value and predictability

Yanjie Cheng · Youmin Tang · Peter Jackson · Dake Chen · Xiaobing Zhou · Ziwang Deng

Received: 21 July 2009 / Accepted: 16 December 2009
© Springer-Verlag 2010

Abstract This is the second part of the 148 years (1856–2003) singular vector analysis, as an extension of part I (Cheng et al. 2009 Clim Dyn, doi:10.1007/s00382-009-0595-7), in which a fully physically based tangent linear model has been constructed for the Zebiak-Cane model LDEO5 version. In the present study, relationships between the singular values and prediction skill measures are investigated for the 148 years. Results show that at decadal/interdecadal time scales, an inverse relationship exists between the singular value (S1) and correlation-based skill measures whereas an in-phase relationship exists between the S1 and MSE-based skill measures. However, the S1 is not a good measure or predictor of prediction skill at shorter time scales such as the interannual time scale and for individual prediction. To explain these findings, S1 was decomposed into linear perturbation growth rate (L1) and linearized nonlinear perturbation growth rate (N1), which are controlled by the opposite underlying model dynamical processes (the linear warming and the nonlinear cooling). An offsetting effect was found between L1 and N1, which have opposite contributions to the S1 (i.e., S1 $\approx$ L1 $-$ N1). The "negative" perturbation growth rate $-$N1 (denoted as NN1) probably is the consequence of the unrealistic nonlinear cooling in the LDEO5 model. Although the correlations of the actual prediction skill to both the L1 and the NN1 are good, their opposite signs lead to a weak relationship between S1 and actual prediction skill. Therefore, either L1 or N1/NN1 is better than S1 in measuring actual prediction skill for the LDEO5 model.

Keywords ENSO · Predictability · Singular vector analysis · Potential predictability measure

Y. Cheng · Y. Tang (✉) · P. Jackson · X. Zhou · Z. Deng
Department of Environmental Science and Engineering, University of Northern British Columbia, 3333 University Way, Prince George, BC V2N 4Z9, Canada
e-mail: ytang@unbc.ca

D. Chen
Lamont-Doherty Earth Observatory of Columbia University, Palisades, NY 10964, USA

D. Chen
State Key Laboratory of Satellite Ocean Environment Dynamics, Hangzhou, China

Present Address:
X. Zhou
Centre for Australian Weather and Climate Research (CAWCR), Bureau of Meteorology, 700 Collins St, Melbourne, VIC 3001, Australia

1 Introduction

El Niño and the Southern Oscillation (ENSO) predictability displays multiple time scales in numerical models, including the seasonal, interannual, and decadal/interdecadal time scales. On the seasonal time scale, ENSO forecast skills in many models decline significantly in the boreal spring with apparent skill recovery in subsequent seasons, showing the "spring barrier" phenomenon (e.g., Jin et al. 2008). On the interannual time scales (2–7 years), ENSO prediction skills are associated with ENSO phase and ENSO intensity, namely, strong ENSO events have high prediction skills, while the neutral ENSO states have poor prediction skills (e.g., Tang et al. 2005, 2008a, Tang et al. 2005, 2008a); The growth phases of both the warm and cold events are better predicted than the corresponding decaying phases in many coupled ENSO forecast models (e.g., Jin et al. 2008). These features of ENSO predictability also occur in the Zebiak-Cane model (Zebiak and

Published online: 07 January 2010

Cane 1987; Chen et al. 2004; hereafter ZC); for example, the warm and cold events are equally predictable while near normal conditions are harder to predict (Chen and Cane 2008). On the decadal/interdecadal time scales, ENSO predictability has apparent decadal/interdecadal variations (e.g., Wang 1995; Kirtman and Schopf 1998; Latif et al. 1998; Chen et al. 2004; Tang et al. 2008a). Tang et al. (2008a) explored ENSO predictability using three models and long term retrospective predictions. Consistent results and conclusions were found in the three models with different complexity, namely, higher prediction skills for the late 19th century and late 20th century, and lower skills for the period of 1916-1955. These consistent relationships found in the three models offer valuable insight to some important issues of ENSO predictability on the longer time scales.

Typically, there are two hypotheses responsible for the loss of predictability with forecast lead time. The first argues that the loss of predictability is due to the chaotic behavior of the nonlinear dynamics of the coupled system (e.g., Jin et al. 1994; Chen et al. 2004), whereas the second attributes it to the stochastic nature of the coupled system characterized by weather noise and other high-frequency variations, such as westerly wind bursts and the Madden–Julian oscillation (e.g., Kirtman and Schopf 1998; Penland and Sardeshmukh 1995; Kleeman and Moore 1997; Moore and Kleeman 1999; Vecchi 2003; Moore et al. 2006; Gebbie et al. 2007; Jin et al. 2007). It is still not clear to date which regime plays the dominant role in controlling the variation of ENSO predictability.

Singular vector analysis (SV) is a powerful tool to study predictability because the optimal perturbation growth suggests the intrinsic limits of prediction skill. The SV has been widely used to study the loss of ENSO predictability due to initial error/perturbation growth (i.e., Lorenz 1965; Chen et al. 1997; Xue et al. 1997a, 1997b; Fan et al. 2000; Tang et al. 2006; Zhou et al. 2008). These SV analyses showed that the perturbation growth rate (i.e., singular value) is sensitive to the seasonal cycle, ENSO phase, and ENSO signals. However, all of the above studies focused on a period of only 20–40 years, with a rather limited number of ENSO cycles, basically precluding statistically robust conclusions. In theory, an inverse relationship could be expected between the leading growth rate and the ENSO predictability. Due to a lack of long term retrospective prediction and corresponding SV analysis, however, the relationship between the singular value and ENSO predictability has not been sufficiently addressed, and especially has not been validated by actual prediction skill measures in previous SV studies. Chen et al. (2004) performed a retrospective forecast experiment spanning the past 148 years, using only reconstructed SST data for model initialization. At a 6-month lead, the model was able to predict most of the warm and cold events occurred during this long period, especially for the relatively large ENSO events. Using the long-term reconstructed SST data and the ZC model LDEO5 version, we recently completed a long-term SV analysis and corresponding retrospective ENSO prediction for the period from 1856 to 2003. In part I of this work (Cheng et al. 2009), we constructed a fully physically based tangent linear model (TLM) for the ZC model, explored the variations of singular vectors and singular values in the time scales from seasons to decades, and examined the control factors responsible for SV variations over the 148 years. A robust and stable optimal perturbation growth pattern and the optimal perturbation growth rate for the 148 years were obtained in part I (Cheng et al. 2009), which could be useful indicators of predictability. To extend this work, the present study focuses on exploring the relationships between the optimal perturbation growth rate, a potential measure of predictability which does not make use of observations, and ENSO actual prediction skills that do make use of observation, for the 148 years at multiple time scales ranging from the interannual time scale to decadal/interdecadal time scale. The identified relationship has a theoretical contribution to predictability study using SV, and a practical significance in estimating the confidence that we can place in future predictions using the same ENSO forecast model.

In Sect. 2, we present a brief introduction to the LDEO5 model and the metrics used to measure actual ENSO prediction skill. The relationships between these prediction skill metrics and the perturbation growth rates are discussed in Sects. 3 and 4. The relationships between the actual prediction skill, perturbation growth rate, and ENSO signals are analyzed in Sect. 5, followed by a conclusion and discussion in Sect. 6.

2 Methods

2.1 ZC model

The model used in this study is the ZC model (Zebiak and Cane 1987) LDEO5 version. The ZC model has been widely applied for ENSO simulation and prediction over two decades, with the latest version of LDEO5 developed in 2004 (Chen et al. 2004). For long retrospective predictions, historic SST of the past 148 years from 1856 to 2003 has been assimilated into the coupled model using a nudging scheme (Chen et al. 2004). The skillful retrospective predictions initialized by the historic SST data, as shown in Chen et al. (2004) and Tang et al. (2008a), are evidence of the good quality of SST initial conditions.

The atmospheric dynamics follows Gill (1980) using steady-state, linear shallow-water equations. The

circulation is forced by a heating anomaly which depends on the SST anomaly and moisture convergence. The ocean dynamics uses the reduced-gravity model, and ocean currents were generated by spinning up the model with monthly wind. The thermodynamics describe the SST anomaly and heat flux exchange. The model time-step is 10 days. The spatial region is focused on the tropical Pacific Ocean (124°E–80°W; 28.75°S–28.75°N); The grid for ocean dynamics is 2° longitude × 0.5° latitude, and the grid for SST physics and the atmospheric model is 5.625° longitude × 2° latitude.

A fully physically based tangent linear model (TLM) was constructed for the LDOE5 model and singular vector analysis performed for the 148-year period from 1856 to 2003, as shown in Cheng et al. (2009). From the long-term SV analyses, the leading singular value (S1) that represents the optimal perturbation growth rate of forecast SSTA, the linear component of S1 (denoted by L1), and the nonlinear component of S1 (denoted by N1) for the 148 years have been obtained. L1/N1/S1 was calculated in the region (11°S–11°N, 129°E–84°W), covering the equatorial tropical Pacific Ocean. We will use these perturbation growth rates as the potential predictability measures to investigate their relationship with several actual prediction skill measures for the LDEO5 model. The actual prediction skill metrics are discussed in Sect. 2.2.

2.2 Metrics of actual prediction skill

Traditionally, the actual prediction skill of ENSO is measured by anomaly correlation coefficient (R) and the mean square error (MSE) between predicted the Nino3.4 SSTA index (averaged over 5°N–5°S, from 170°W to 120°W) against the observed counterpart.

$$R(t) = \frac{\sum_{i=1}^{N} \left[T_i^{\mathrm{p}}(t) - \mu^{\mathrm{p}}\right]\left[T_i^{\mathrm{o}}(t) - \mu^{\mathrm{o}}\right]}{\sqrt{\sum_{i=1}^{N} \left[T_i^{\mathrm{p}}(t) - \mu^{\mathrm{p}}\right]^2}\sqrt{\sum_{i=1}^{N} \left[T_i^{\mathrm{o}}(t) - \mu^{\mathrm{o}}\right]^2}} \quad (1)$$

$$\mathrm{MSE}\,(t) = \frac{1}{N-1}\sum_{i=1}^{N}\left(T_i^{\mathrm{p}}(t) - T_i^{\mathrm{o}}(t)\right)^2 \quad (2)$$

where T is the index of NINO3.4 SSTA, t is the lead time of the prediction from 1 to 12 months, T^{p} is the predicted NINO3.4 SSTA, and T^{o} is corresponding observed counterpart, subscript i the initial time of prediction ($i = 1,\ldots,N$); μ^{p} is the mean of the forecasts, μ^{o} is the mean of observations. N is the number of samples used over 148 years in this study, a total of 148 × 12 ($N = 1{,}776$) forecasts, initialized from January 1856 to December 2003, were run starting at 1 month interval (1 January, 1 February…1 December), and continued for 12 months for the ZC model. SST assimilation was used to initialize the forecasts as discussed in Chen et al. (2004). The seasonal cycle has always been removed from forecasts and observations prior to measuring prediction skill. To evaluate an individual prediction skill, the mean square error of individual prediction (MSEIP) is used for all leads up to 12 months, as defined in Tang et al. (2008a, b),

$$\mathrm{MSEIP}_i = \frac{1}{12}\sum_{t=1}^{t=12}\left(T_i^{\mathrm{p}}(t) - T_i^{\mathrm{o}}(t)\right)^2 \quad (3)$$

2.3 Cross-wavelet analyses

The Cross-wavelet transform (XWT) method is used for examining relationships between two time series in time–frequency space (e.g., Grinsted et al. 2004). From the XWT analysis, the common power and relative phase can be revealed. The phase differences between two variables are depicted by the direction of a vector, with in-phase pointing right, anti-phase pointing left, and the first variable leading the second by 90° pointing straight down. In this study, a continuous XWT technique with the Morlet wavelet as the mother function was applied. Monte Carlo methods are used to assess the statistical significance against a red noise background. The standard software package of cross-wavelet transform is available online (http://www.pol.ac.uk/home/research/waveletcoherence). Further details on XWT analysis can be found in Grinsted et al. (2004) and Torrence and Compo (1998).

3 The singular value and ENSO predictability

As a potential predictability measure, the optimal perturbation growth rate (S1) presumably has an inverse relationship to the actual model prediction skill, namely, when S1 is large, the predictability is low and vice versa. Such a perception has been applied in studying potential predictability of ENSO using the theory of optimal perturbation growth (e. g., Moore and Kleeman 1998; Moore et al. 2006; Tang et al. 2006). However, the relationship between S1 and the actual prediction skill measures such as the anomaly correlation (R) and mean square error (MSE) to date has not been well examined due to a lack of long-term retrospective ENSO predictions and corresponding SV analysis, as discussed in the introduction. Different from previous SV studies, we will focus on discussing relationship for individual forecasts rather than an overall feature, which offers useful potential metric in estimating the performance of a forecast when verification data is absent. In the next section, the relationships between singular value and actual prediction skill metrics will be investigated at various time scales for the period of 148 years from 1856 to 2003.

3.1 S1–predictability relationship on the decadal/interdecadal time scale

Firstly, we examine the relationship between the perturbation growth rate S1 and the ENSO prediction skills at the decadal/interdecadal time scales. All the skill measures presented in Sect. 2 are used, including anomaly correlation (R), MSE, and MSEIP. The correlation preliminarily evaluates the phase differences between the forecasts and observations, while the MSE and MSEIP quantify the amplitude departure between the forecasts and the observations. Unless otherwise indicated, the predicted and observed Nino3.4 SSTA indices are used to evaluate these actual prediction skills in this study. The S1 was calculated with the optimal period of 9-months. As found in Cheng et al. (2009), the fastest perturbation growth rate (maximum S1) occurs at a 9-month lead in the LEDO5 model. Correspondingly, the prediction correlation skill and MSE skill vary slowly with lead time after 9-month leads (Chen et al. 2004; Chen and Cane 2008). This motivates us to choose the S1 of 9-month lead in the following discussions.

To examine the relationship of S1 to predictability on the interdecadal time scales, a running window of 25-year was applied to the S1 and the actual prediction skill measures, namely that, they were evaluated at each window of 25 years, starting from January 1856 and moving forward by 1 month each time until December 2003. Since R and MSE are a function of lead time, their values averaged over lead times of 1–12 months are presented in Fig. 1. As can be seen in Fig. 1, on the interdecadal time scale over the 148 years, there is an inverse relationship between the S1 and the correlation skill (R) and an in-phase relationship between S1 and the MSE. These relationships are consistent with the conventional concept of S1 and predictability, namely, when the S1 is small, prediction skill was good, i.e., high correlation skill R and small MSE-based skill; whereas when the S1 was large, the opposite situation occurs. Note that the averaged MSEIP over a running window is equivalent to the averaged MSE over all lead times, as suggested by (2) and (3).

The running mean method used above may not be able to present objectively a full spectrum of the relationship between S1 and predictability; for example, the relationship is probably sensitive to the length of running window. To explore the decadal/interdecadal relationships, further we extract low-frequency components using the fast Fourier transform (FFT) filter. Shown in Fig. 2a are low-frequency components of S1 and the MSEIP, obtained by a 10-year low-pass FFT filter. Generally, Fig. 2a confirms the in-phase relationship in Fig. 1b, with a significant positive correlation coefficient of 0.4 over the 148 years between the S1 and MSEIP. A further scrutiny to Fig. 2a reveals that the in-phase relationship has decadal/interdecadal variation. Figure 2b shows the correlation coefficient between the filtered S1 and MSEIP, computed using the running window of 25 years over the 148 years. As can be seen, the in-phase relationship between S1 and MSEIP was much stronger during the late nineteenth and twentieth centuries than during the periods from 1910 to 1920 and 1940 to 1955. In following discussions, we will see that the in-phase relationship between S1 and predictability is most probably due to decadal variation in ENSO signals.

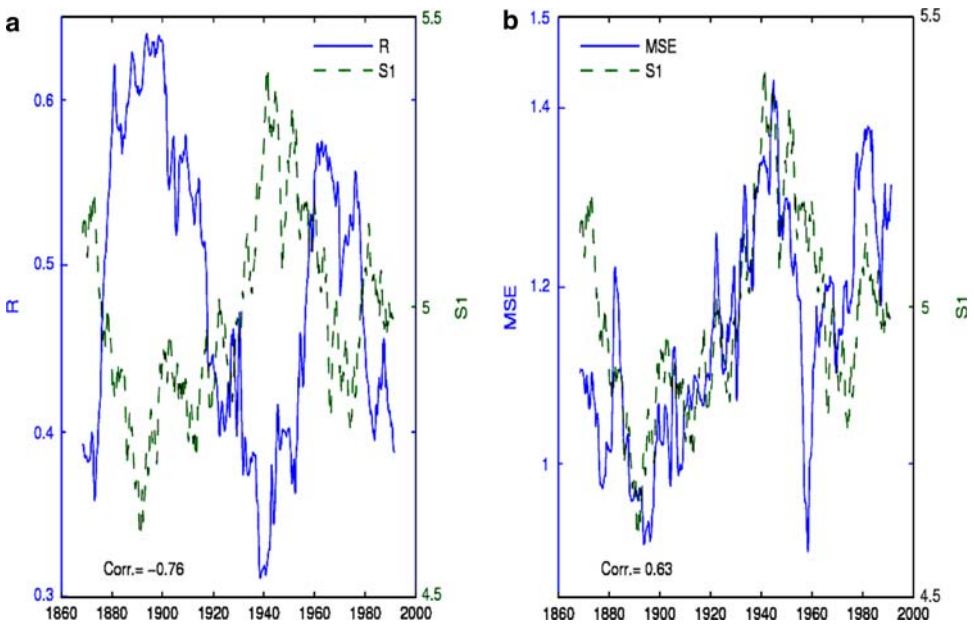

Fig. 1 Interdecadal variations of (**a**) anomaly correlation coefficient (R) and the singular value (S1); (**b**) MSE and S1. A 25-year running window was applied on all data at each month from January 1856 to December 2003. MSE measures are averaged over lead times of 1–12 months

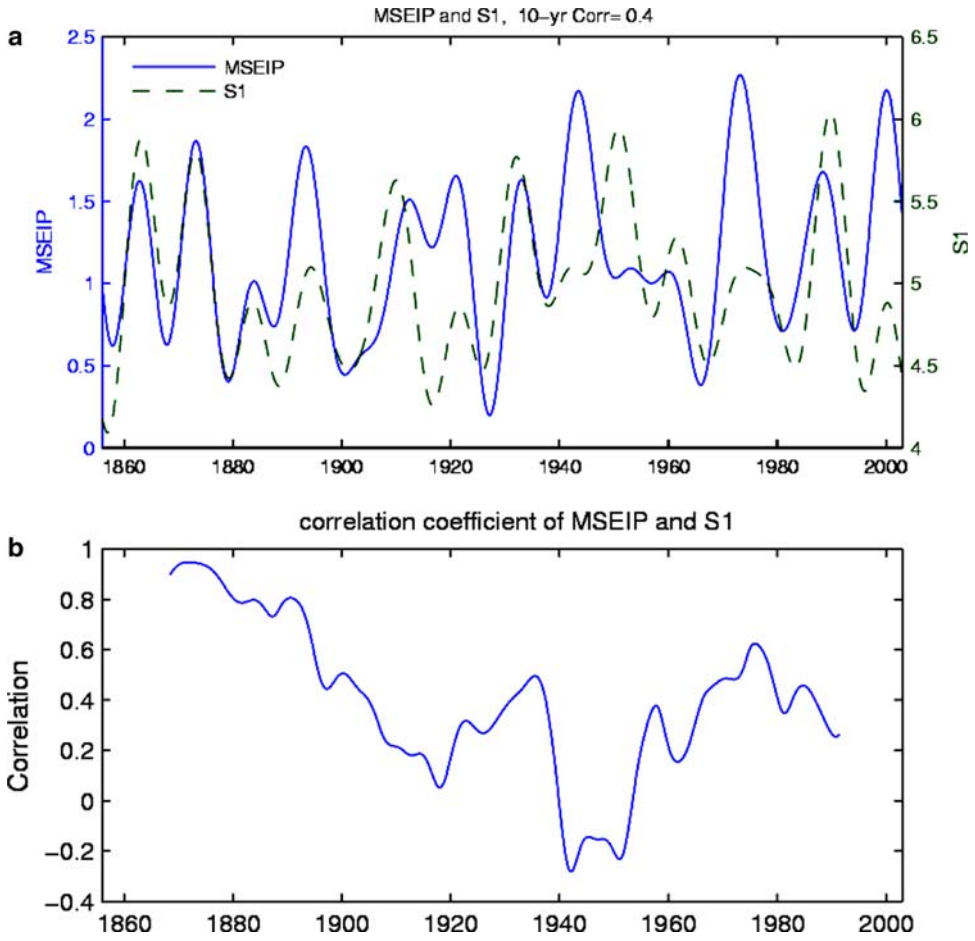

Fig. 2 **a** Decadal/interdecadal variations of MSEIP and singular value (S1). A 10-year low-pass FFT filter method was applied on these skill measures. **b** Temporal variations of the correlation coefficient between S1 and MSEIP over the 148 years, correlation coefficients were calculated in a 25-year running window

3.2 S1–predictability relationship on interannual time scales

In the proceeding section, an in-phase relationship was found between the S1 and MSE skill metric at long time scales greater than decade. A further analysis explores whether such an in-phase relationship exists at interannual time scales and for individual forecast cases. Shown in Fig. 3 is the scatter plot of S1 against MSEIP, where a 2–7 year FFT filter has been applied to both variables to extract their interannual variability. Figure 3 indicates large uncertainties in the relationship between S1 and MSEIP, suggesting that, on the interannual time scales, the optimal error growth rate S1 might not be a good indicator of actual model skill.

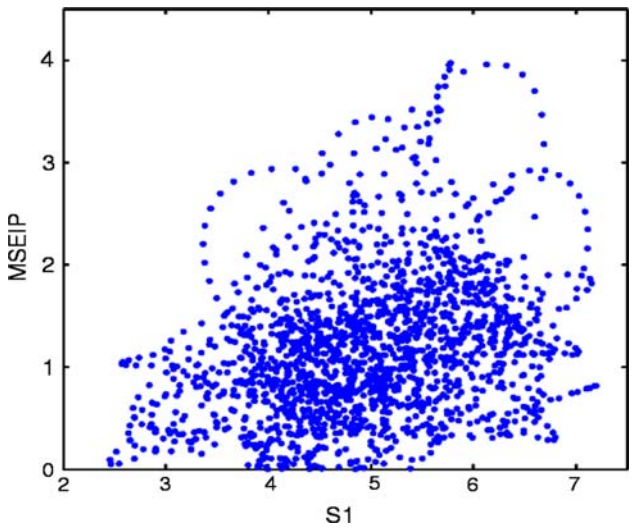

Fig. 3 The relationships between the singular value S1 and the actual predictability measures at interannual time scales using a 2–7-year FFT filter. The S1 against MSEIP

3.3 S1–predictability relationship on all time scales

For all time scales ranging from seasons to decades, the relationship between S1 and predictability is measured using all original samples without filtering, as shown in Fig. 4 and the second column of Table 1. Here, MSE and R were evaluated in a period as a function of lead time, making them unavailable in Table 1. As shown in Fig. 4, a large uncertainty exists in the relationship between S1 and MSEIP, with a low correlation value of 0.16.

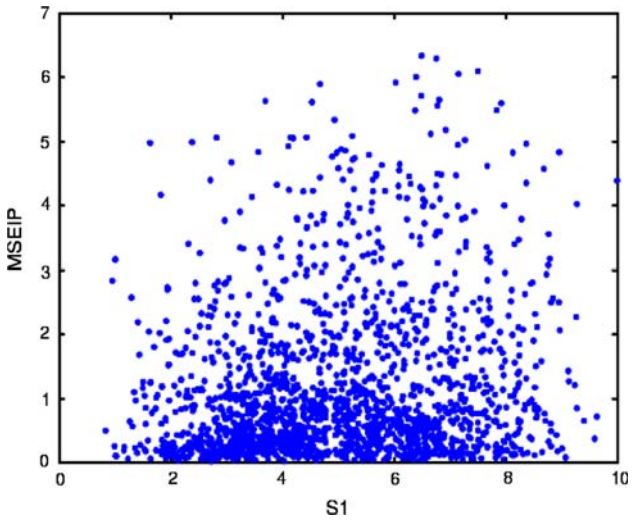

Fig. 4 Same as Fig. 3 but for all time scales without using an FFT filter

Table 1 Correlation coefficients of potential predictability measures and actual predictability measure

	S1	L1	NN1	LH	NH
MSEIP	0.16	0.33	−0.36	0.58	−0.51

The actual predictability measure is MSEIP, whereas the potential predictability measures include the leading singular value (S1), the linear perturbation growth rate (L1) and the nonlinear perturbation growth rate (NN1). The LH and NH represent the linear heating and nonlinear heating items in SST governing equation, averaged over the NINO3.4 region and over the optimal period of 12 months

In summary, the relationship between S1 and predictability is complex, dependent on time scales and the target of evaluation. At decadal time scales, S1 has an in-phase relationship to MSE and an inverse relationship to correlation skill; whereas at interannual time scales and for individual forecasts, the relationships between S1 and prediction skill measures have larger uncertainties. Thus S1 might not be the best indicator of predictability. In next section, we will further explore S1 and propose a better measure for quantifying potential predictability.

4 The linear/nonlinear perturbation growth rates and the actual predictability

As analyzed in the proceeding section, there are significant uncertainties in the relationship between S1 and predictability at interannual time scales and for individual initial conditions. Conceptually, a good relationship between them should be expected since S1 quantitatively measure the fastest error growth. However, the potential predictability measure S1 is the fastest error growth rate, which might not always indicate the actual predictability in the actual forecasts. Thus, it is interesting to explore additional possible reasons responsible for the uncertainties of S1 and actual predictability, in particular, to identify better measures of potential predictability than S1.

Practically, the perturbation growth, denoted by δS, can be decomposed into the perturbation growth due to the linear heating (LH), δL, and that due to the nonlinear heating[1] (NH), δN, namely;

$$\delta S = \delta L + \delta N \tag{4}$$

δS, δL, and δN are the final perturbation growth at the lead time of 9-month, obtained by the TLM with the SV1 as the initial perturbations. Cheng et al. (2009) found that there is a strong inverse relationship (with a correlation coefficient of -0.81) between δL and δN in the central and eastern Pacific; the linear perturbation growth δL is about twice as large as δN in amplitude, and δN is always negative whereas δL is positive in most time. Thus, the strong inverse relationship between linear and nonlinear perturbation growth can be approximately depicted as below

$$\delta N \approx b\delta L, \tag{5}$$

where b is a constant value with $-1 < b < 0$.

Applying the L-2 norm on (5) and (4), respectively, we have

$$\|\delta N\| \approx |b| \cdot \|\delta L\| = -b\|\delta L\|. \tag{6}$$

$$\begin{aligned}\|\delta S\| &= \|\delta L + \delta N\| = \|\delta L + b\delta L\| + \Delta S \\ &= (1+b)\|\delta L\| + \Delta S = \|\delta L\| + b\|\delta L\| + \Delta S\end{aligned} \tag{7}$$

In (7), the ΔS is the residual term arising from the approximations in (5) and (6), representing the perturbation growth due to the interaction of linear and nonlinear heating. The value of 1 + b is always positive due to of the condition $-1 < b < 0$. Thus,

$$\|\delta S\| = \|\delta L\| - \|\delta N\| + \Delta S \tag{8}$$

Based on the definition of perturbation growth rate (singular value), the total optimal perturbation growth rate S1 can be decomposed into the contribution of LH (referred to as linear growth rate L1) and the contribution of NH (referred to as nonlinear growth rate N1), given by (8), namely,

$$\mathrm{S1} = \mathrm{L1} - \mathrm{N1} + \Delta S = \mathrm{L1} + \mathrm{NN1} + \Delta S, \tag{9}$$

where NN1 = −N1, a negative value representing a negative/offsetting contribution of NH to S1. In following

[1] Note that the nonlinear heating term has been linearized in the TLM, thus the nonlinear perturbation growth used in this paper, unless otherwise indicated, means the perturbation growth due to the nonlinear heating term linearized in the TLM.

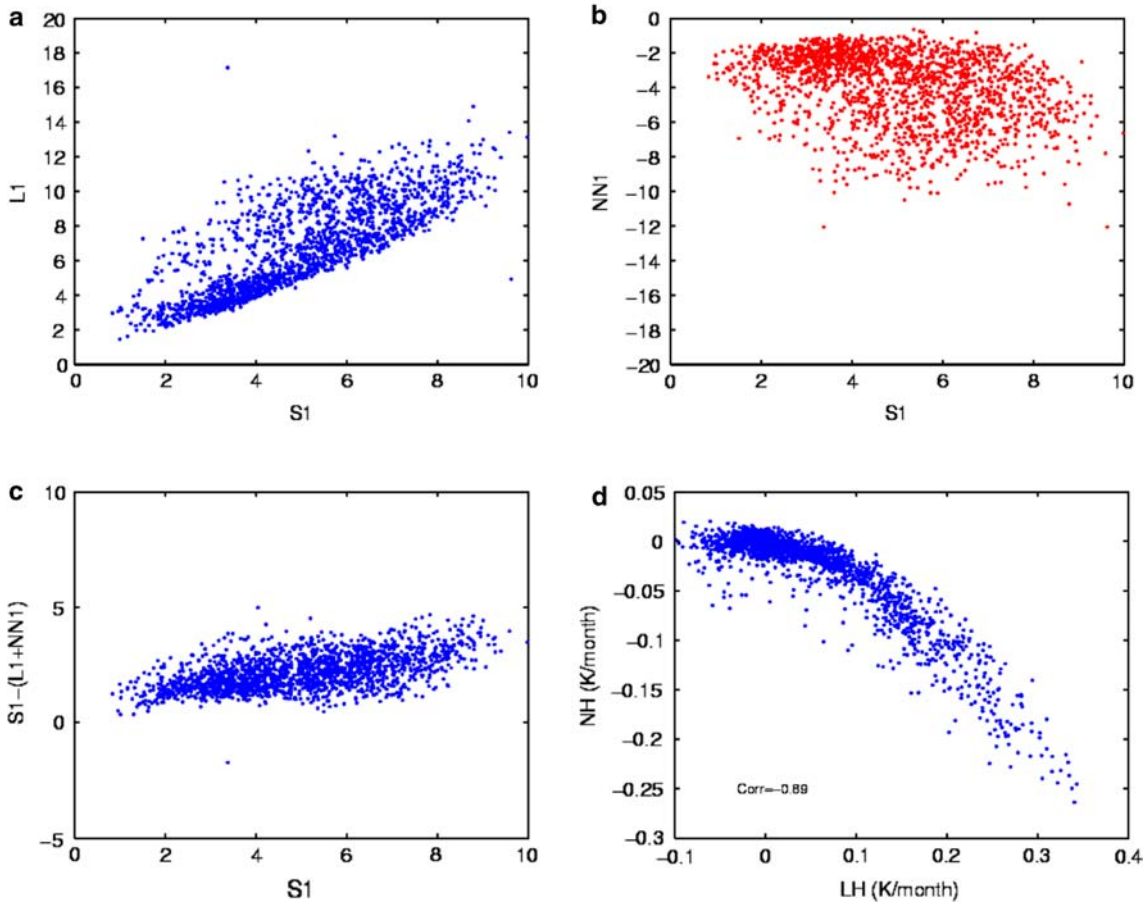

Fig. 5 Scatter plots between (**a**) LH and NH (K/month). And the relationships of the linear (L1), nonlinear (NN1), and the total (S1) perturbation growth rates. **b** L1 against S1. **c** NN1 against S1. **d** S1-(L1 + NN1) against S1

analysis, we will find that the ΔS is small compared with L1 and NN1.

Shown in Fig. 5a–c are scatter plots of L1, NN1 and ΔS against S1 for the period from 1856 to 2003; where ΔS is obtained by S1 − (L1 + NN1). As can be seen, the contribution of ΔS to S1 is rather small (ranging from 0 to 5 with the mean value of 2.0 in Fig. 5c), and S1 is mainly determined by the sum of the perturbation growth rates L1 and NN1. Figure 5a–c indicates that L1 and NN1 have an offset effect or an opposite contribution on S1, i.e., a positive relationship between L1 and S1 in contrast to an inverse relationship between NN1 and S1. Such an offsetting effect might be a preliminary reason why S1 is not a good indicator of actual prediction skill as found above. In other words, either L1 or NN1 might be expected to have a better relationship with actual prediction skills than S1.

A strong anti-correlation between L1 and NN1 stems from the underlying dynamical processes (i.e., linear heating LH and nonlinear heating NH) as argued above. To illustrate the strong inverse relationship between LH and NH, a scatter plot of NH against LH is given in Fig. 5d, where the LH/NH is the averaged linear/nonlinear heating at the NINO3.4 region over the lead times from 1 to 9 months for individual forecasts. A strong inverse correlation between LH and NH is visible with a significant correlation coefficient value of −0.89. As seen in Fig. 5d, the LH mainly has a warming effect in about 72% of forecasts for the 148 years, whereas the NH always contributes to a cooling effect. The cooling effect of the NH becomes stronger as the warming effect of LH increases, leading to a strong offsetting effect between LH and NH in most cases. Due to the strong offsetting effect in the underlying dynamical processes, the total heating (LH + NH) has a poor relationship with the total error growth S1 with a small correlation coefficient of 0.13.

Table 1 shows the correlation coefficients between the actual prediction skill MSEIP and potential predictability measure L1/NN1 (the third and fourth column). As can be seen, both L1 and NN1 have stronger relationships to prediction skills than S1, indicating NN1 or L1 to be a better measure of potential predictability in the ZC model. A comparison between these correlation coefficients reveals that the L1 and NN1 have opposite relationships to predictability, as displayed by a positive correlation

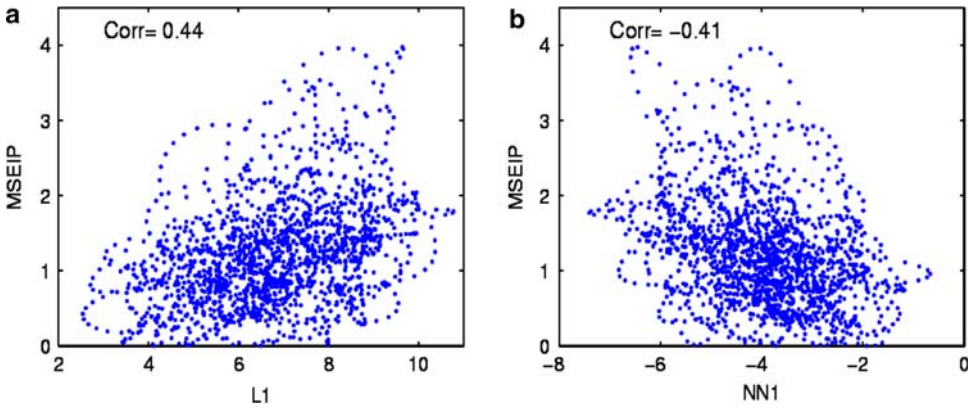

Fig. 6 The relationships between the linear/nonlinear singular values and the prediction skill MSEIP at interannual time scales using a 2–7-year FFT filter. **a** L1 against MSEIP; **b** NN1 against MSEIP

coefficient for L1 but a negative value for NN1. This offset effect might explain well why there is a relatively small correlation value between S1 and predictability as shown in Table 1. From the sign of correlation coefficients, one can infer that the positive S1–MSEIP relationship is mainly determined by the positive L1–MSEIP relationship.

Shown in Fig. 6 are scatter plots of L1 and NN1 against the prediction skill MSEIP. Like Fig. 3, a 2–7 year FFT filter was applied here for each variable to address interannual time scales. In contrast to the large uncertainties in the relationship of S1–predictability as shown in Fig. 3, Fig. 6 shows visible relationship of L1/NN1–predictability. The correlation coefficients between L1/NN1 and prediction skills are all statistically significant at the confidence level of 95%, as shown in the upper-left corner of each panel. An opposite relationship between L1–MSEIP and NN1–MSEIP can be observed in Fig. 6, showing an offset effect of L1 and NN1 on predictability, as found earlier in Table 1. Thus, Fig. 6 explains the large uncertainties in S1–predictability in Fig. 3, and also indicates that either L1 or NN1 is a better measure of potential predictability than S1.

A further analysis is placed on the relationship between the LH/NH and actual prediction skill. Table 1 includes the correlation coefficients between the averaged LH/NH over the optimal period of 9 months and the actual prediction skill. As shown in the fifth and sixth columns of Table 1, LH and NH significantly correlate with MSEIP, namely, when LH/NH is strong, the MSEIP skill is large and vice versa. Again, the NH has always a cooling effect as aforementioned, thus the negative sign of its correlation coefficient in Table 1 imply the link of stronger cooling and the larger MSEIP. This explains the relationships between the L1/NN1 and the prediction skill. These results are in agreement with our previous findings that both the model linear/nonlinear perturbation growth rate and the linear/nonlinear heating term are controlled by the underlying linear/nonlinear processes, respectively (Cheng et al. 2009).

To illustrate the time-scale-dependent characteristics of the relationship between perturbation growth rates and MSEIP, we performed cross-wavelet analyses for them as shown in Fig. 7. The in-phase relationship is presented by arrows pointing right, whereas the anti-phase (or inverse) relationship is displayed by arrows pointing left. The thick contour encloses regions of greater than 95% confidence, using a red-noise background spectrum. Several features can be revealed by Fig. 7. First, the scale-dependent feature of the S1–MSEIP relationships is seen in Fig. 7a. At longer time scales >10 years, a strong in-phase relationship is displayed in the S1–MSEIP for the periods of 1860–1940 and 1970–2000 (Fig. 7a), which is in agreement with the decadal variations of correlation coefficients in Fig. 2b. At shorter time scales <10 years, wavelet analysis reveals additional scale-dependent relationships. For example, at 6–10 years time scale, anti-phase relationships are shown in two time periods of 1890–1910 and 1970–1980, which are opposite to the in-phase relationships displayed at decadal/interdecadal time scales. For 2–6 years time scale, in-phase relationships occurred again but confined in 1860–1900 and around 1960. This scale-dependent relationship is consistent with the results shown in Sect. 3. Second, at all time scales, the S1–MSEIP relationship (Fig. 7a) looks more like the L1–MSEIP relationship (Fig. 7b) than the NN1–MSEIP (Fig. 7c). This similarity is because that the contribution of LH to SSTA is about twice as much as the NH (Cheng et al. 2009), thereby the original S1–MSEIP relationship is mainly determined by the L1–MSEIP relationship. Third, at interannual time scales, the L1 (NN1) shows a more frequently consistent in-phase (anti-phase) relationship with MSEIP, suggesting L1 or NN1 is a better measure than S1. Furthermore, the NN1–MSEIP relationship (Fig. 7c) is consistently inverse for almost over all the time scales. It does not have the scale-dependent feature like that in S1-skill (Fig. 7b) and L1-skill (Fig. 7b), where in-phase and anti-phase relationship change alternatively from time to time. This unique feature of the NN1-skill relationship suggests that NN1 is a more reliable measure

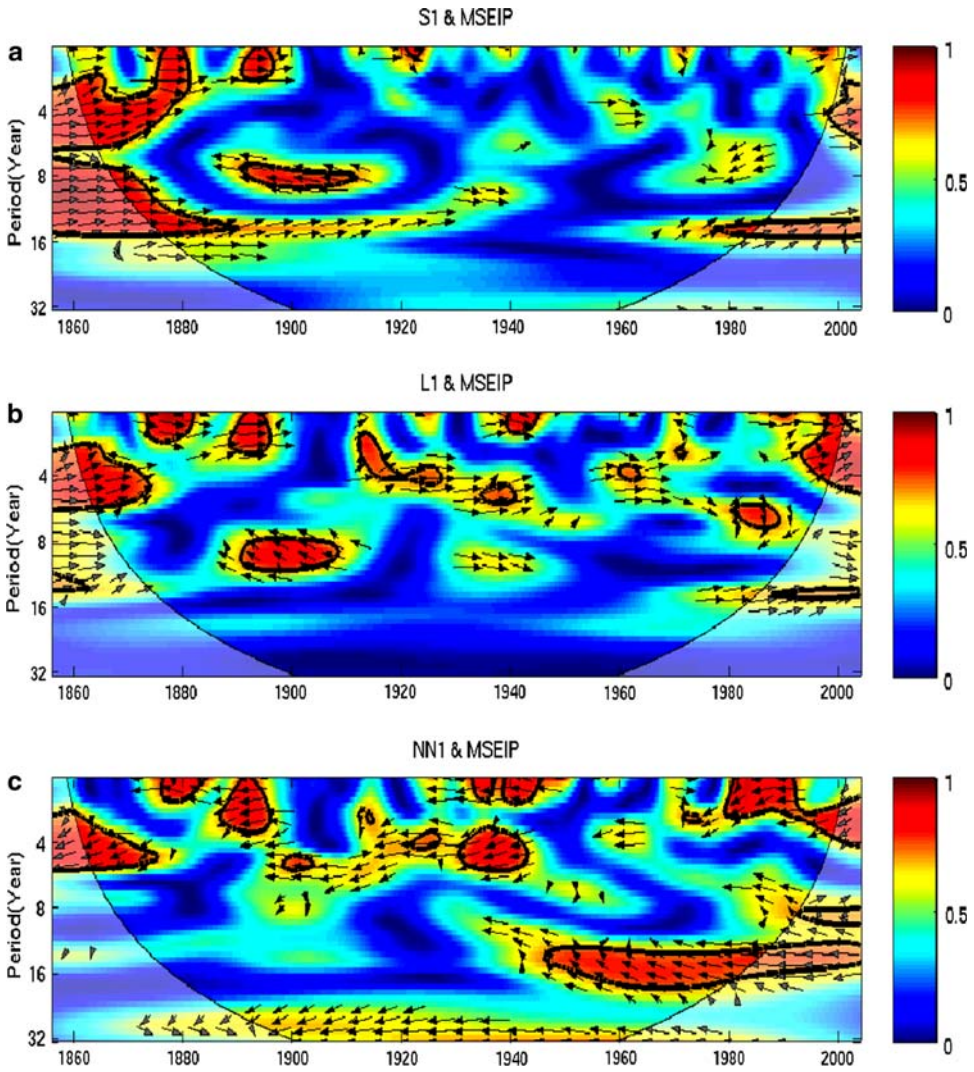

Fig. 7 The cross-wavelet analysis for the singular values S1/L1/NN1 and actual prediction skill MSEIP. (**a**) S1 and MSEIP; (**b**) L1 and MSEIP; (**c**) NN1 and MSEIP. The thick contour encloses regions of greater than 95% confidence, using a red-noise background spectrum. The relative phase relationship is shown as arrows, with in-phase pointing right, anti-phase pointing left, and singular values leading skills by 90° pointing straight down. (A 2-year FFT filter was applied on all data before performing the cross-wavelet analyses)

of potential predictability. It should be noted that the NH has much smaller contribution to SSTA, but NN1 has a consistently significant anti-phase relationship with MSEIP skill at all time scales, suggesting that a strong negative perturbation growth is related to a large MSEIP. Another feature shown in Fig. 7 is that, at interannual time scale, the L1 and NN1 brings a strong offsetting effect on MSEIP (opposite arrow direction) during the period from 1910 to 1960, leading to a large uncertainty in the relationship between S1 and MSEIP as shown in Fig. 3.

5 ENSO signals, the optimal error growth rates, and predictability

It has been suggested in many recent studies that ENSO predictability is strongly associated with signal components present in initial fields (e.g., Peng and Kumar 2005; Tang et al. 2005, 2008a; Moore et al. 2006). Often, a stronger ENSO event is easier to predict than a neutral event. At the decadal/interdecadal time scales, Tang et al. (2008a) compared retrospective ENSO predictions of 120 years from three models and found that, at the decadal/interdecadal time scales, high correlation skills often occurred at the time periods with strong ENSO events whereas low correlation skills occurred at weak ENSO periods. The positive relationship between ENSO signals and the correlation skill was explained in Kleeman (2002), Tang et al. (2005), and Tang et al. (2008a), using information theory. They argued that the extra information provided by the forecast, called prediction utility, is highly associated with the signals present in the initial conditions. As the ENSO signal is stronger, more extra information will be produced compared with the climatological forecast, which leads to a more skillful and reliable forecast. However, the ENSO signal and predictability at shorter

time scales, i.e., interannual time scales, has not been well addressed. In this section, we will examine relationships between the ENSO signal and the optimal growth rates at time scales ranging from interannual time scale to decadal/interdecadal time scales.

An inverse relationship has been suggested between the optimal perturbation growth and the intensity of ENSO variability, in some recent SV and breeding vector analyses: a small perturbation growth rate S1 often occurs during an ENSO peak phase, and the larger perturbation growth rate S1 appears in the neutral and onset/breakdown stages of ENSO (Chen et al. 1997; Xue et al. 1997b; Tang et al. 2005; Cai et al. 2003; Zhou et al. 2008; Cheng et al. 2009). These works identified the inverse relationship either using a comparison of the maximum S1 against the intensity of ENSO variability or using an analytical solution of the delay oscillator model.

A metric to measure the intensity of the ENSO signal should be defined. Tang et al. (2008a) proposed three measures to quantify the intensity of ENSO over a time period including: (1) the variance of NINO3.4 SSTA index, (2) the variance of the first EOF mode, and (3) total spectrum power at frequencies of 2–5 years. Tang et al. (2008a) shows that the three measures produce similar decadal/interdecadal variation of ENSO signal. In Part I of this work (Cheng et al. 2009); ENSO signal was defined by the absolute value of NINO3.4 SSTA index. In the present study, we use the same definition to measure the intensity of ENSO signal to be consistent with Part I.

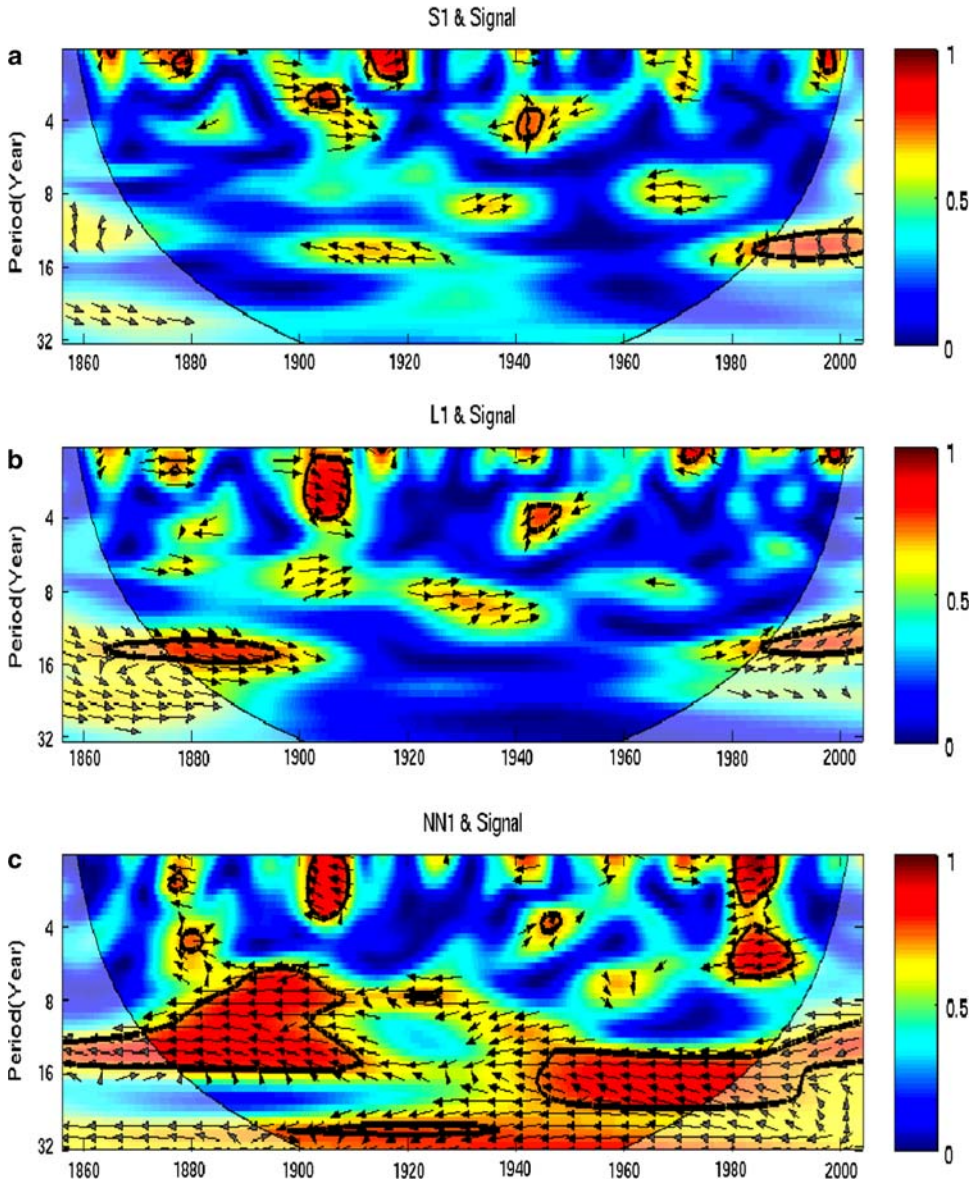

Fig. 8 The cross-wavelet analysis for ENSO signal (|NINO3.4|) and the singular values S1, L1, and NN1

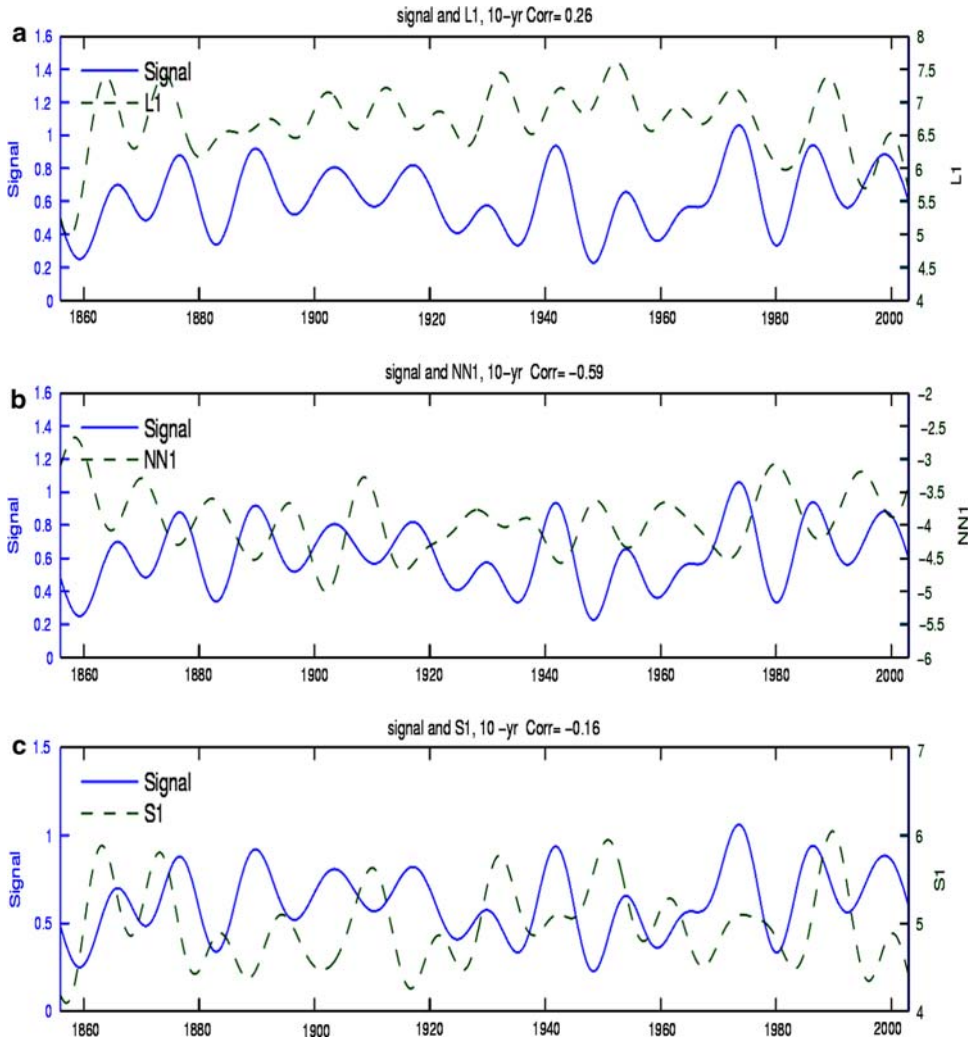

Fig. 9 Decadal/interdecadal variations of ENSO signal (|NINO3.4|; the solid line) and perturbation growth rates (dash lines): (**a**) the linear perturbation grow rate (L1); (**b**) the linearized nonlinear perturbation growth rate (NN1); (**c**) the total perturbation growth rate S1. A 10-year low-pass filter has been applied

The relationships between S1/NN1/L1 and ENSO signals are displayed in Fig. 8 using cross-wavelet analyses. At the decadal/interdecadal time scales, the L1 and NN1 have stronger relationships to ENSO signals than the S1, especially for the period from 1880 to 1910 and around 1980. This is especially true for the NN1–signal relationship which holds for almost all the periods from 1880 to 1980. At the decadal/interdecadal time scales, the S1–signal relationship in Fig. 8a is determined by both L1 and NN1. As can be seen, the anti-phase NN1–signal relation cancels the in-phase L1–signal relationship completely in 1860–1900 and partly in the 1980s and later. Therefore, both L1 and NN1 have important contributions to the original S1–signal relationship at decadal/interdecadal time scales. These features are furthered revealed in plots of variations in S1/NN1/L1 against signal as shown in Fig. 9.

On the interannual time scales, the relationship between S1 and ENSO signals is not clear in Fig. 8a. The in-phase and anti-phase relationships occur randomly from decade to decade. On the other hand, for most periods during the 148 years, the L1–signal and NN1–signal show consistently good in-phase and anti-phase relationship, namely, a strong ENSO signal is associated with a large L1 (small NN1) while a weak ENSO signal corresponds with a small L1 (large NN1). Especially, the NN1–signal relationship is most significant during the 148 years at both decadal and interannual time scales.

The relatively good relationship between NN1/L1 and ENSO signals can be further demonstrated in the plots of variations in NN1/L1/S1 against ENSO signals. Shown in Fig. 9 are these variations at decadal time scale. As can be seen, a much better relationship between NN1 and ENSO signals can be identified, which explains the importance of nonlinear heating in ENSO variability and predictability as found in other studies (e.g., Tang and Deng 2009; Cheng et al. 2009). For interannual time scale, we also found that the ENSO signal is more related to NN1 than to others (not shown).

6 Conclusion

In this study, we investigated ENSO predictability using the optimal perturbation growth and long-term retrospective hindcasts using the ZC model. Emphasis was placed on exploring the relationship between potential predictability measured by the optimal perturbation growth rates and actual hindcast skill for long-period from 1856 to 2003. A good measure of potential predictability is useful practically because it can estimate the prediction skill without using the observations, and offer a practical means of estimating the confidence level of an individual prediction.

To find the best measure of potential predictability, three metrics obtained from SV analyses in part I of this work (Cheng et al. 2009) have been examined at different time scales, including the leading singular value S1, the linear (L1) and linearized nonlinear (N1) components of S1. The L1 and N1 reflect the optimal perturbation growth of the linear and nonlinear heating terms in the SST governing equation of the ZC model. The measures of actual prediction skill include correlation coefficient, MSE, and mean square error of individual prediction (MSEIP). Generally, at decadal/interdecadal time scales, our findings from the long-period analysis of 148 years confirmed the theoretical perception that S1 has an inverse relationship with correlation-based skill, and a positive relationship with MSE-based skills. However, at shorter time scales, e.g., interannual time scales, and for individual forecast cases, there are large uncertainties in the relationship between S1 and actual prediction skills, which prevents the S1 from being a good measure of potential predictability.

Several reasons are probably responsible for the small correlation between S1 and actual predictability. First, S1 is a collective error growth jointly contributed by the linear and nonlinear processes. A strong inverse relationship between LH and NH might cause an unrealistic offsetting contribution to S1, as indicated by strong anti-correlation between L1 and NN1, biasing the relationship between S1 and prediction skill. Instead, L1 or NN1, removing the offsetting influence, might better characterize the relationship between potential skill and actual skill. Second, S1/L1/NN1 is a potential measure, and represents the optimal/fastest error growth rate but such an extreme situation does not always happen in the realistic forecasts. Therefore, even under the perfect model scenario, they still may not have a very good relationship with the actual predictability. S1 represents a more extreme situation than NN1 and L1 since it contains L1, NN1, probably leading to worse relationship to actual skill. Third, the relationship between potential and actual skill is also influenced by model bias inherent to model internal dynamics and physical processes. The model is always not perfect. The S1 involves more physical processes than either L1 or NN1, thus the model bias can more easily impact S1 than L1/NN1, more biasing the relationship between potential predictability and actual prediction skill.

An important finding in this work is that the linear/nonlinear perturbation growth rate L1 and NN1 are better measures of potential predictability than the optimal perturbation growth rate S1 in terms of the capability of estimating the actual prediction skills. Among the three potential measures, NN1 has a consistent relationship with actual prediction skills for all time scales. Uncertainty in the relationship between S1 and prediction skill measure is due to an offsetting effect of linear heating and nonlinear heating on the optimal perturbation growth, causing an opposite relationship between L1–predictability and NN1–predictability.

A practical application of this study is to use L1 and NN1 to characterize potential predictability. It was also found that the residual term in Eq. (9) has small contribution to the S1, allowing to use the sum of L1 and NN1 to replace S1. The analysis of L1 and NN1 can be applied to all time scales and is suitable for individual cases and overall features. It should be noted that a high correlation skill and a large MSE value can occur simultaneously, namely one prediction is good in phase but poor in magnitude. This is most probably due to the nature of prediction target whose variance is large. It is well recognized that strong El Niño events might be easier to predict than normal events but the prediction errors in amplitude often are larger for strong ENSO events. Thus, it might be necessary to draw conclusions and summarize findings from the two different predictability measures.

The perturbation growth rate L1/NN1 depends on the nature of initial conditions and the internal dynamical processes (i.e., linear and nonlinear heating). The latter often controls the intensity of ENSO variability. Due to the offsetting effect of linear and nonlinear heating on ENSO variability and the time-scale dependent nature of these dynamical processes, the relationship between S1 and ENSO signals depends on both the time periods and time scale (e.g., Fig. 8). For example, an inverse relationship can be identified on the interannual time scales over the recent decades (after 1960s), consistent with those documented in previous BV and SV studies. However, this inverse relationship does not hold well for other periods and for other time scales. In contrast to the uncertain S1–signal relationship, the NN1 shows a consistent inverse relationship with ENSO signals for all periods and time scales.

Several cautions should be borne in mind. First, the SV analyses and retrospective hindcasts are often model-dependent, suggesting that the results and conclusion drawn from this work might not be generalized. More models are required to fully generalize these conclusions. Second, some physical processes are either simplified or

missing in the ZC model. For example, stochastic atmospheric noise is not considered in this model. Stochastic forcing has been thought to be a main source to limit ENSO predictability. Thus, the predictive skill shown in the ZC model might be a lower bound of ENSO actual prediction skill (Chen and Cane 2008). Third, the total nonlinear heating NH always contributes to a cooling effect in the ZC model, which is opposite to the observation as discussed in An and Jin (2004) where the vertical nonlinear warming dominates the total nonlinear heating term. This is due mainly to model unrealistic simulation of the zonal current anomaly. Thus, some results found in this work may be model dependent. However, the unrealistic simulation of NH is common in current ENSO prediction models. Comparing nonlinear heating terms in ten coupled models reveals that only one model gave the correct simulation of NH and others fail to represent both the location and strength or even the sign of the nonlinear vertical warming (An et al. 2005). Fourth, the results and conclusions in this study might be also dependent on the metrics of actual prediction skill. In this study, we explored ENSO predictability using correlation-based and MSE-based measures, especially MSEIP. When the chosen metrics have been widely used in the field of predictability study, they might not be able completely characterize all properties of predictability. Finally, we used a running window of 25-year to analyze interdecadal variations in predictability and other variables. The window length of 25-year was arbitrary and subjective although several sensitivity experiments with different window lengths did not essentially change the aforementioned results. These concerns need to be addressed through more comprehensive analyses.

Nevertheless, this work explored ENSO statistical predictability over the past 148 years, providing insights on ENSO predictability, especially offering a practical means to estimate the confidence level for individual forecasts for the ZC model. An investigation of individual error growth rates, i.e., the linear perturbation growth L1 and the nonlinear perturbation growth N1 from their controlling processes (the underlying linear and nonlinear advections) offer the better potential measures for ENSO predictability. Since the perturbation growth L1 and N1 are determined by the underlying linear and nonlinear dynamical processes, respectively, these processes are fundamental reasons that contribute to the strong relationships of signal/perturbation growth and ENSO predictability. For example, the relationship between N1 and forecast skill probably is the result of two known relationship: (1) relation between ENSO magnitude and forecast skill, (2) relation between the nonlinear heating and ENSO magnitude.

Acknowledgments This work is supported by Canadian Foundation for Climate and Atmospheric Sciences (CFCAS) GR7027. Yanjie Cheng is also supported by the Graduate fellowship of NSERC PGS D2-362539-2008. Dake Chen is supported by research grants from National Basic Research Program (2007CB816005) and National Science Foundation of China (40730843). We would like to thank two anonymous reviewers for their constructive comments and suggestions.

References

An S, Jin F-F (2004) Nonlinearity and asymmetry of ENSO. J Clim 17:2399–2412

An S, Ham YG, Kug JS, Jin FF, Kang IS (2005) El Niño–La Niña asymmetry in the coupled model intercomparison project simulations. J Clim 18:2617–2627

Cai M, Kalnay E, Toth Z (2003) Bred vectors of the Zebiak–Cane Model and their potential application to ENSO predictions. J Clim 16:40–56

Chen D, Cane MA (2008) El Niño prediction and predictability. J Comput Phys 227:3625–3640

Chen YQ, Battisti DS, Palmer RN, Barsugli J, Sarachik E (1997) A study of the predictability of tropical Pacific SST in a coupled atmosphere/ocean model using singular vector analysis. Mon Weather Rev 125:831–845

Chen D, Cane MA, Kaplan A, Zebiak SE, Huang D (2004) Predictability of El Niño over the past 148 years. Nature 428:733–736

Cheng Y, Tang Y, Zhou X, Jackson P, Chen D (2009) Singular vector and ENSO predictability in a coupled model—a further analysis of Lamont Model from 1856-2003, part I: singular vector and the control factors. Clim Dyn. doi:10.1007/s00382-009-0595-7

Fan Y, Allen MR, Anderson DLT, Balmaseda MA (2000) How predictability depends on the nature of uncertainty in initial conditions in a coupled model of ENSO. J Clim 13:3298–3313

Gebbie G, Eisenman I, Wittenberg A, Tziperman E (2007) Modulation of westerly wind bursts by sea surface temperature: a semistochastic feedback for ENSO. J Atmos Sci 64:3281–3295

Gill AE (1980) Some simple solutions for heat-induced tropical circulation. Q J R Meteorol Soc 106:447–462

Grinsted A, Moore JC, Jevrejeva S (2004) Application of the cross wavelet transform and wavelet coherence to geophysical time series. Nonlinear Process Geophys 11:561–566

Jin F-F, Neelin JD, Ghil M (1994) El Niño on the devil's staircase: annual subharmonic steps to chaos. Science 264:70–72

Jin F-F, Lin L, Timmermann A, Zhao J (2007) Ensemble-mean dynamics of the ENSO recharge oscillator under state-dependent stochastic forcing. Geophys Res Lett 34:L03807. doi:10.1029/2006GL027372

Jin EK, Kinter JL III, Wang B, Park CK, Kang IS, Kirtman BP, Kug JS, Kumar A, Luo JJ, Schemm J, Shukla J, Yamagata T (2008) Current status of ENSO prediction skill in coupled ocean–atmosphere model. Clim Dyn 31:647–664

Kirtman BP, Schopf PS (1998) Decadal variability in ENSO predictability and prediction. J Clim 11:2804–2822

Kleeman R (2002) Measuring dynamical prediction utility using relative entropy. J Atmos Sci 59:2057–2072

Kleeman R, Moore AM (1997) A theory for the limitation of ENSO predictability due to stochastic atmospheric transients. J Atmos Sci 54:753–767

Latif M, Anderson D, Barnett T, Cane M, Kleeman R, Leetma A, O'Brien J, Rosati A, Schneither E (1998) A review of the predictability and prediction of ENSO. J Geophys Res 103(C7):14375–14393

Lorenz EN (1965) A study of the predictability of a 28-variable atmospheric model. Tellus 17:321–333

Moore AM, Kleeman R (1998) Skill assessment for ENSO using ensemble prediction. Q J R Meteorol Soc 124:557–584

Moore AM, Kleeman R (1999) Stochastic forcing of ENSO by the intraseasonal oscillation. J Clim 12:1199–1220

Moore AM, Zavala-Garay J, Tang Y, Kleeman R, Weaver AT, Vialard J, Sahami K, Anderson DLT, Fisher M (2006) On the low-dimensionality of ENSO as evidenced by the optimal forcing patterns of coupled models. J Clim 19:4683–4699

Peng P, Kumar A (2005) A large ensemble analysis of the influence of tropical SSTs on seasonal atmospheric variability. J Clim 15:1068–1085

Penland C, Sardeshmukh PD (1995) The optimal growth of tropical sea surface temperature anomalies. J Clim 8:1999–2024

Tang Y, Deng Z (2009) Low-dimensional nonlinearity of ENSO and its impact on predictability. Phys Dyn. doi:10.1016/j.physd.2009.11.006

Tang Y, Kleeman R, Moore A (2005) On the reliability of ENSO dynamical predictions. J Atmos Sci 62(6):1770–1791

Tang Y, Kleeman R, Miller S (2006) ENSO predictability of a fully coupled GCM model using singular vector analysis. J Clim 19:3361–3377

Tang Y, Deng Z, Zhou X, Cheng Y, Chen D (2008a) Interdecadal variation of ENSO predictability in multiple models. J Clim 21:4811–4833

Tang Y, Lin H, Moore A (2008b) Measuring the potential predictability of ensemble climate predictions. J Geophys Res 113:D04108. doi:10.1029/2007JD008804

Torrence C, Compo GP (1998) A practical guide to wavelet analysis. Bull Am Meteorol Soc 79(1):61–78

Vecchi GA, Harrison DE (2003) On the termination of the 2002–03 El Niño event. Geophys Res Lett 30, 1946. doi:10.1029/2003GL017564

Wang B (1995) Interdecadal changes in El Niño onset in the last four decades. J Clim 8:267–285

Xue Y, Cane MA, Zebiak SE (1997a) Predictability of a coupled model of ENSO using singular vector analysis, part I: optimal growth in seasonal background and ENSO cycles. Mon Weather Rev 125:2043–2056

Xue Y, Cane MA, Zebiak SE (1997b) Predictability of a coupled model of ENSO using singular vector analysis, part II: optimal growth and forecast skill. Mon Weather Rev 125:2057–2073

Zebiak SE, Cane MA (1987) A model El Niño-Southern Oscillation. Mon Weather Rev 115:2262–2278

Zhou X, Tang Y, Deng Z (2008) The impact of nonlinear atmosphere on the fastest error growth of ENSO prediction. Clim Dyn 30:519–531. doi:10.1007/s00382-007-0302-5